Int. J. Electrochem. Sci., 15 **(2020)** 11623 – 11631, doi: 10.20964/2020.11.29

International Journal of
ELECTROCHEMICAL
SCIENCE
www.electrochemsci.org

Short Communication

rGO-Co-MoS_2 Composite as Highly Active Electrocatalysts for Hydrogen Evolution Reaction

Guang Zhao[1], Shun Wang[1], Gaoliang Zhou[1], Shengjie Sun[1], Zhengyu Yang[1], Jianguo Lv[1,2,] ,Yuxuan Ma[1], Ying Wang[1], Changjuan Hu[1], Junjun Zhang[1], Jin Yang[1], Gang He[3,*], Miao Zhang[2, 3], Min Zhao[1,2], Xiaoshuang Chen[4], Lei Yang[5]*

[1] School of Physics and Materials Engineering, Hefei Normal University, Hefei 230601, China
[2] Key Laboratory for Photoelectric Detection Science and Technology of Education Department of Anhui Province, Hefei Normal University, Hefei 230601, China
[3] School of Physics and Material Science, Anhui University, Hefei 230039, China
[4] National Laboratory for Infrared Physics, Shanghai Institute of Technical Physics, Chinese Academy of Sciences, Shanghai 200083, China
[5] Department of Chemistry and Materials Engineering, Hefei University, Hefei 230601, China
[*]E-mail: lvjg1@163.com (J. Lv), hegang@ahu.edu.cn (G. He)

Received: 12 July 2020 / *Accepted:* 24 August 2020 / *Published:* 30 September 2020

MoS_2, Co-MoS_2 and rGO-Co-MoS_2 were synthesized successfully by a simple hydrothermal method. microstructures and Raman spectra of the samples were investigated by X-ray diffraction analysis and Raman spectroscopy. The result indicate that the peaks at 14.4°, 33.0° and 58.4° may be assigned to (002), (100) and (110) plane of pure MoS_2, respectively. The crystallinity of MoS_2 may be restrained by cobalt doping. D band and G band of amorphous carbon can be seen in the rGO-Co-MoS_2. XPS result indicated that the rGO-10-Co-MoS_2 is mainly consisted of S, Mo, Co, C and O, respectively. The electrochemical performance test results show that rGO-10-Co-MoS_2 presents the lowest overpotentials of 205 mV at a current density of 10 mA cm^{-2} and the smallest Tafel slope, indicating cobalt doping and rGO hybrid can improve electrocatalytic activity for HER. In addition, The sample also exhibit good electrocatalytic stability in the acid condition.

Keywords: rGO-Co-MoS_2; Hydrothermal synthesis; Hydrogen evolution reaction;

1. INTRODUCTION

The excessive use of fossil fuels aggravates air pollution and global warming. Therefore, it is increasingly urgent to develop a clean and renewable fossil fuel alternative[1]. In the strategic research of developing alternative energy, building energy infrastructure with hydrogen as the main carrier and

providing cheap and clean energy will become the direction of future efforts [2]. Because water is a rich and renewable hydrogen source, electrolyzed water provides hope for sustainable hydrogen production and technical support for hydrogen energy regeneration. However, the high cost of electrolyzed water limits the industrial application of this technology [3]. In the past few decades, with the increase of population, automobiles and energy appliances, the demand for energy has increased dramatically, resulting in a large consumption of fossil fuels[4]. Hydrogen is the best fuel for the next generation of clean and renewable energy[5]. Electrochemical technology is one of the existing efficient hydrogen production technologies[6-8]. At present, the commercial electrocatalysts for hydrogen production are mainly precious metals such as platinum (Pt), and the development of high-efficiency electrocatalysts composed of abundant elements on earth will significantly reduce the cost of electrocatalysis[9, 10]. In recent years, researchers have developed excellent non noble metal catalysts and achieved fruitful results through breakthroughs in the field of nanoscience and nanotechnology. Among them, molybdenum disulfide is the most representative catalyst in the transition metal sulfide[11]. Because of its unique layered structure and electrochemical activity, its application in the field of electrocatalytic water decomposition has been widely concerned and has been explored as potential alternatives for HER [11-14]. It's called typical Graphene-based materials due to their structure and properties [15-17]. MoS_2 is widely used photocatalytic and electrocatalytic studies of hydrogen evolution reactions (HER) [18].

In this paper, pure MoS_2, Co-MoS_2, and rGO-Co-MoS_2 power were prepared via simple hydrothermal process. The samples were designed as a work electrode and electrocatalytic performance have been tested by the three-electrode electrochemical workstation (CHI660E) in 0.5mol/L H_2SO_4 solution. Compared to MoS_2 and Co-MoS_2 power, the rGO-Co-MoS_2 exhibits superior electrocatalytic performance.

2. EXPERIMENTAL

2.1. Preparation of sample

All chemical reagents with analytical purity were used without further purification. In a typical synthesis of MoS_2, 240mg thioacetamide and 120mg sodium molybdate dehydrate were dissolved in 40 mL of deionized water. Then, the mixed solution was transferred into a 50 mL Teflon-lined stainless steel autoclave, which was maintained at 220 °C for 24 h. After the reaction, the autoclave drops to room temperature. The final products were washed with water and absolute ethanol for several times and dried at 60 °C for 24 h. The Co-MoS_2 sample was synthetized by adding 58mg cobalt nitrate hexahydrate in the process of MoS_2 synthesis. The rGO-5-Co-MoS_2, rGO-10-Co-MoS_2 and rGO-20-Co-MoS_2 samples was prepared by adding 5mg, 10mg and 20mg graphene oxide in the preparation of Co-MoS_2 samples, respectively.

2.2. Characterization

The microstructure of samples were measured by means of X-ray diffraction analysis (XRD, TD-3500) with the Cu$K\alpha$ radiation (λ=1.5418 Å) at 30 kV and 40 mA. Raman spectra of the samples were

investigated on a Raman spectroscopy (inVia-Reflex, Renishaw). Surface morphology of samples were tested by field emission scanning electron microscopy (FE-SEM, S-4800). Chemical components and valence states were characterized by X-ray photoelectron spectroscopy (XPS, Thermo, ESCALAB 250).

2.3. Electrochemical measurements

Electrochemical performance tests were carried out on an electrochemical workstation(CHI660E) with a standard three-electrode system, which composed of a catalyst coated carbon paper working electrode, an Ag/AgCl reference electrode and a carbon cloth counter electrode. The 10 mg catalyst powder was dissolved in isopropyl alcohol (400 μL) and Nafion (5.0 wt%, 25 μL) solution, and then treated with ultrasound for 60 minutes to form a homogeneous ink. The dispersion was loaded on carbon paper with an area of 1.0×1.0 cm^2..Subsequently, the carbon paper coated with the catalyst was put into a vacuum drying oven at 60 ℃ to dry for 10 hours to obtain the working electrode. The potentials vs. Ag/AgCl were converted to the reversible hydrogen electrode (RHE) using the following relationship[19]:

$$E_{RHE} = E_{Ag/AgCl} + 0.059 \times pH + 0.1976\ V \quad (1)$$

where E_{RHE} is the converted potential vs. RHE and $E_{Ag/AgCl}$ is the experimentally measured potential against Ag/AgCl reference.

The HER polarization curves were tested with a scan rate of 10.0 mV s^{-1} at room temperature in N_2-saturated 0.5mol H_2SO_4, respectively. All potentials were iR-compensated. And the presented current density was normalized to the geometric surface area. All the polarization curves were the steady-state ones after several cycles. The electrochemical impedance spectroscopy (EIS) test was carried out by applying an AC voltage of 5.0 mV amplitude in the frequency range of 10^5 to 0.01 Hz and recorded at -0.3V.

3. RESULTS AND DISCUSSION

Fig. 1 presents the XRD patterns of MoS_2, Co-MoS_2, rGO-5-Co-MoS_2, rGO-10-Co-MoS_2 and rGO-20-Co-MoS_2 samples, respectively. Three characteristic peaks at 14.4°, 33.0° and 58.4° for pure MoS_2 could be attributed to (002), (100) and (110) plane, respectively [8, 20, 21]. Intensity of the characteristic peak for the MoS_2 decreases when cobalt is added. This suggests crystallinity of MoS_2 may be restrained by cobalt doping. The result is similar to those of previous study, which report that the diffraction peak intensity of MoS_2 was inhibited by the addition of grapheme [22]. Addition of rGO has little effect on diffraction peak intensity of MoS_2. In addition, characteristic diffraction peaks from sulfide of cobalt and rGO were not observed in the XRD patterns, which may be owing to the low content and detection limit of instrument. It was confirmed in other subsequent representations.

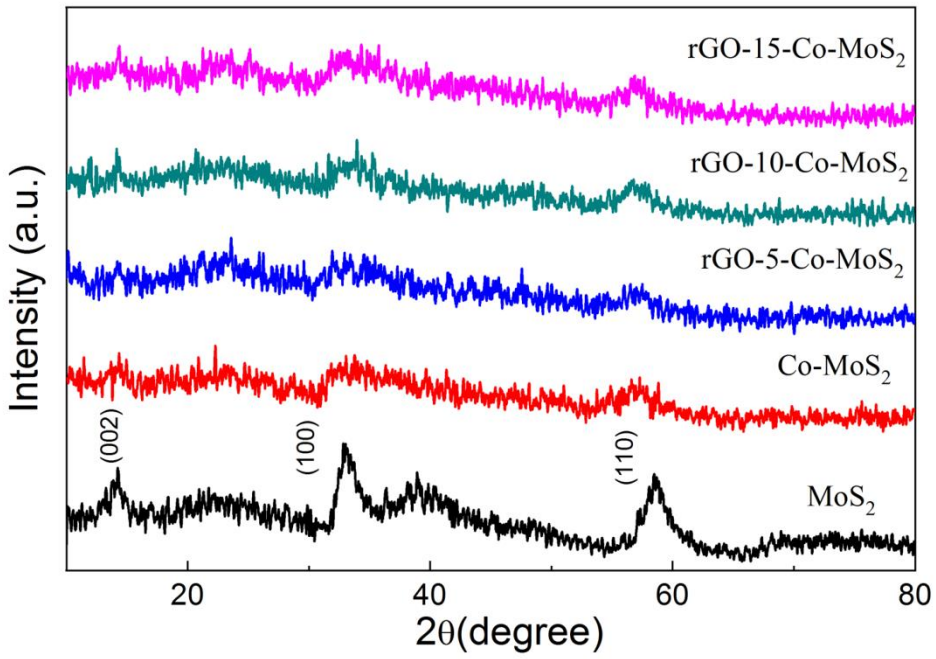

Figure 1. XRD patterns of MoS_2, Co-MoS_2, rGO-5-Co-MoS_2, rGO-10-Co-MoS_2 and rGO-20-Co-MoS_2.

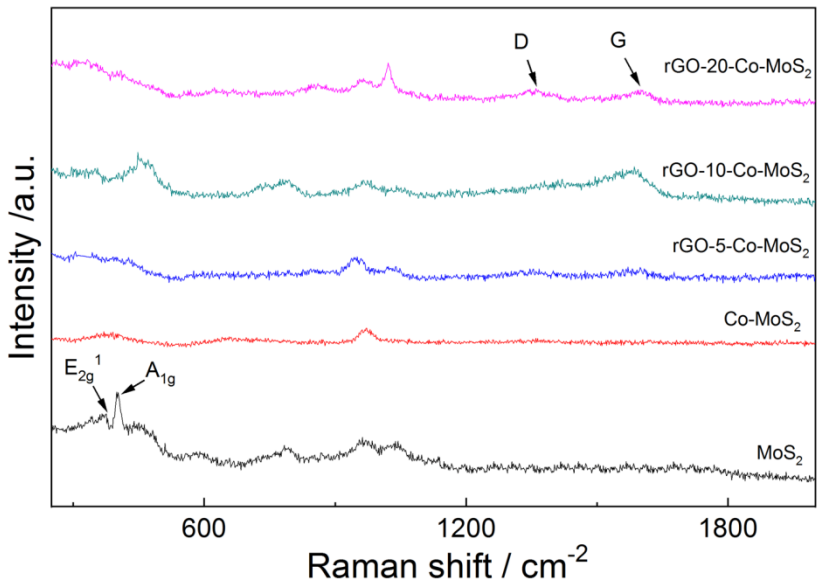

Figure 2. Raman spectra of MoS_2, Co-MoS_2, rGO-5-Co-MoS_2, rGO-10-Co-MoS_2 and rGO-20-Co-MoS_2.

Fig. 2 shows the Raman spectrum of the MoS_2, Co-MoS_2, rGO-5-Co-MoS_2, rGO-10-Co-MoS_2 and rGO-20-Co-MoS_2, respectively. It can be seen that two Raman characteristic peaks for the pure MoS_2 sample at 372 cm^{-1} and at 402 cm^{-1} are indexed to the E^1_{2g} and A_{1g}, which are corresponded to the in-plane vibration phonon mode of Mo-S and the out-of-plane vibration phonon mode of S atoms, respectively [23]. When cobalt is added, the intensity of the Raman characteristic peaks decrease, indicating that the crystallinity of MoS_2 decreases. The incorporation of rGO has little effect on its

Raman characteristic peaks of MoS_2. The results are consistent with the XRD test results. The other two Raman characteristic peaks at about 1369 and 1590 cm^{-2} may be attributed to D and G bands of amorphous carbon, corresponding to the graphitized carbon and disordered carbon. The formation of graphitized carbon will help improve catalyst conductivity and catalytic activity[24].

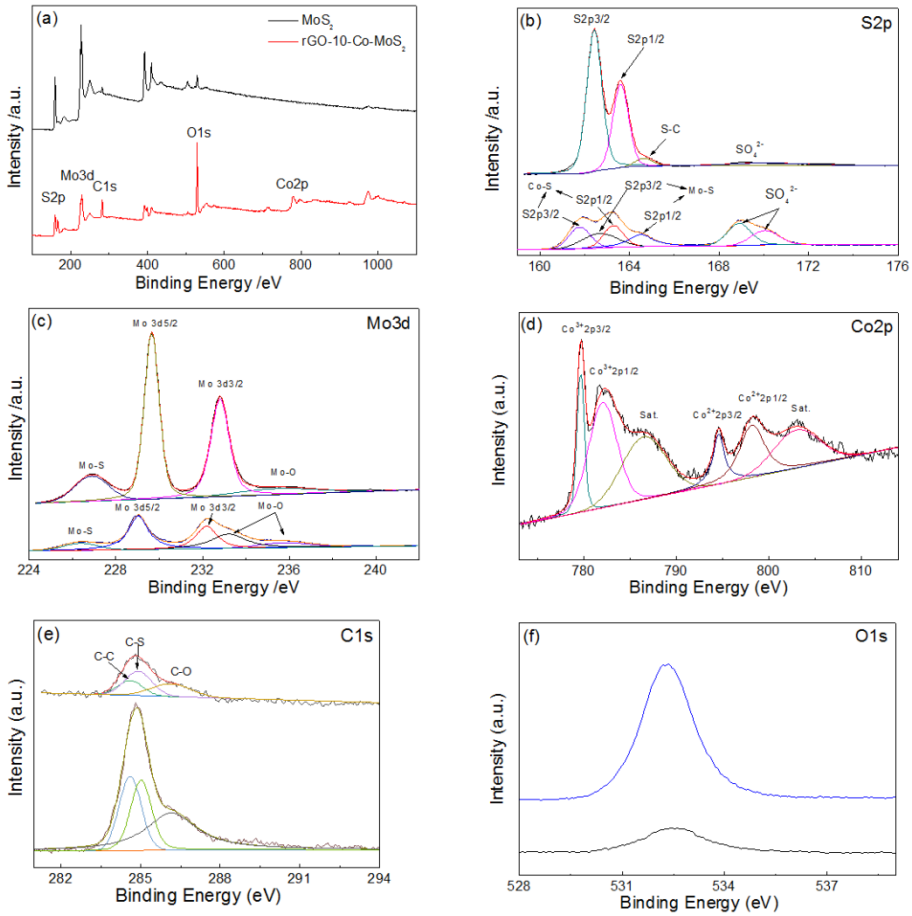

Figure 3. (a) XPS survey spectra and high-resolution XPS spectra of (b) S2p, (c) Mo3d, (d) Co2p, (e) C1s and (f) O1s for MoS_2 and rGO-10-Co-MoS_2.

Fig.3a shows the XPS survey spectrum of MoS_2 and rGO-10-Co-MoS_2. It can be seen that the sample is mainly consisted of S, Mo, Co, C and O. Fig.3b presents high resolution S2p XPS spectra, which can be simulated into several sub-peaks. In the S2p XPS spectrum of MoS_2, two peaks centered at about 162.4 eV and 163.6 eV, corresponding to the S2p3/2 and S2p1/2 binding energies of S^{2-} in MoS_2, respectively[25]. The peaks centered at about 164.7eV and 170.1 eV were attributed to the C-S and SO_4^{2-} species, respectively. In the S2p spectra of rGO-10-Co-MoS_2, the peaks located at 161.7 eV and 163.3 eV may be indexed to the S2p3/2 and S2p1/2 binding energies of Co-S bond [19]. Two peaks at 162.7 eV and 164.5 eV may be assigned to the S2p3/2 and S2p1/2 binding energies of S^{2-} in MoS_2[26]. Two peak centered at 168.8 eV and 170.1 eV are assigned to the SO_4^{2-} species, which may be attributed to partial oxidation of sulfur species. Fig. 3c shows the high-resolution Mo3d spectra for the MoS_2 and

rGO-10-Co-MoS_2, which can be fitted by several sub-peaks. For the MoS_2, two peaks central at 229.6 and 232.8 eV may be indexed to the Mo 3d5/2 and Mo3d3/2 of Mo^{4+}. The peak centered at 235.8 eV is attributed to the MoO_3 due to slight oxidation of the sample surface. The peak centered at 226.8 eV may be attributed to the S2s, corresponding to the S species of Mo-S band [27]. For the rGO-10-Co-MoS_2, two peaks located at about 229.1 and 232.2 eV may be assigned to the Mo 3d5/2 and Mo 3d3/2 of Mo^{4+}, respectively. Two peaks located at 233.2 and 235.8 eV are also be attributed to the MoO_3. The peak located at 226.4 eV is also assigned to the S2s. Due to the strong interaction between rGO and MoS_2, the Mo3d peaks of rGO-10-Co-MoS_2 shift to the lower binding energies compared with MoS_2[26]. Fig.3d provides high-resolution Co2p spectrum of the rGO-10-Co-MoS_2. The Co2p spectrum can be fitted into six sub-peaks. Three peaks centered at 779.6 eV, 782.0 eV and 786.5eV are assigned to Co2p3/2, Co2p1/2 and corresponding satellite peak of Co^{3+}[28]. The other three peaks centered at 794.5 eV, 798.2 eV and 803.0 eV are indexed to Co2p3/2, Co2p1/2 and corresponding satellite peak of Co^{2+}. The results indicated that the cobalt exists in the form of bivalent and trivalent in the rGO-10-Co-MoS_2[29]. Fig.3e shows the high-resolution C1s spectra of the MoS_2 and rGO-10-Co-MoS_2. The C1s peak can be deconvoluted into three peaks with binding energies of 284.6, 284.9and 286.1, corresponding to C–C, C–S and C–O, respectively[26]. Fig.3f presents the high resolution O1s XPS spectra of the MoS_2 and rGO-10-Co-MoS_2. The symmetrical peaks centered at about 532.4 eV may be assigned to the hydroxyl groups on the surface of the samples [30].

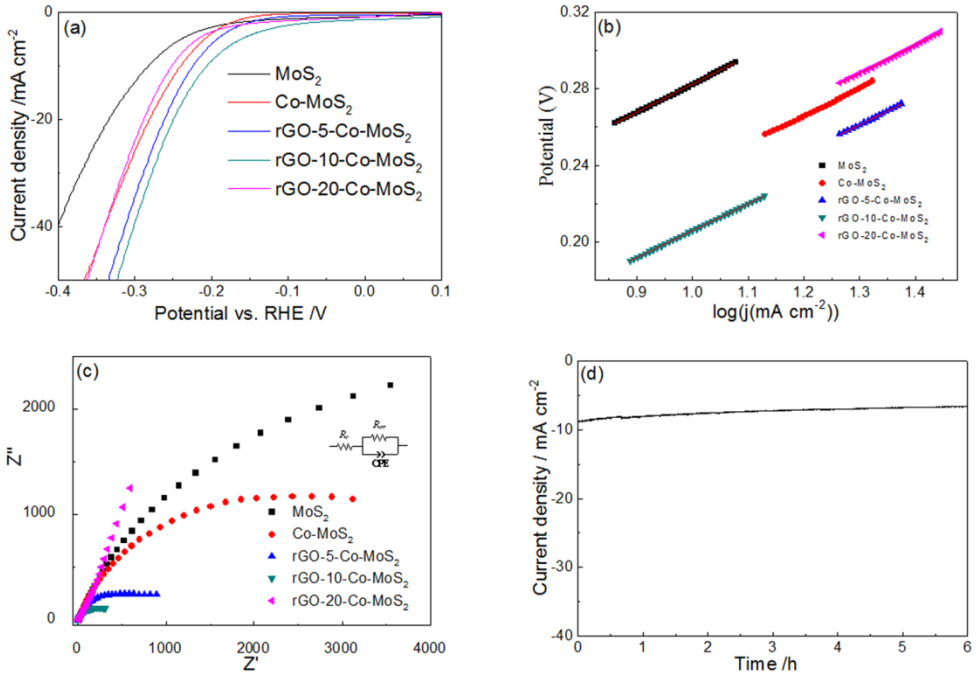

Figure 4. (a) LSV polarization curves of MoS_2, Co-MoS_2, rGO-5-Co-MoS_2, rGO-10-Co-MoS_2 and rGO-20-Co-MoS_2 in 0.5M H_2SO_4 acid environment, respectively; (b) Tafel plots derived from (a); (c) Nyquist plots of MoS_2, Co-MoS_2, rGO-5-Co-MoS_2, rGO-10-Co-MoS_2 and rGO-20-Co-MoS_2 at an overpotential of -0.3V in 0.5M H_2SO_4 solution, the inset shows the equivalent electric circuit model; (d) *I*-t curve of rGO-10-Co-MoS_2 for 6h.

Fig.4a presents the content LSV polarization curves for evaluating the electrocatalytic HER performance of MoS_2, Co-MoS_2, rGO-5-Co-MoS_2, rGO-10-Co-MoS_2 and rGO-20-Co-MoS_2 samples, respectively. The overpotentials at a current density of 10 mA cm^{-2} are 281, 240, 224, 205 and 252 mV, for MoS_2, Co-MoS_2, rGO-5-Co-MoS_2, rGO-10-Co-MoS_2 and rGO-20-Co-MoS_2, respectively. It can be seen that the pure MoS_2 exhibits the inferior electrocatalytic HER performance, while the moderate Co doping can effectively improved MoS_2 HER performance. rGO-10-Co-MoS_2 displays the optimum electrocatalytic HER performance, suggesting that adding appropriate rGO amount in the Co-MoS_2 can effectively regulate the electrocatalytic HER performance. Table 1 compares the performance of our rGO-10-Co-MoS_2 electrocatalyst with several noble metal free HER electrocatalyst. The overpotentials of rGO-10-Co-MoS_2 close to or lower than the results reported in the literature.

Table 1. Summary of the HER catalytic activity of similar electrocatalyst

Electrocatalyst	Electrolyte	Overpotential η (mV)	j (mA·cm-2)	Ref.
rGO-10-Co-MoS_2	0.5M H_2SO_4	205	10	This work
Ni@NC-800	1M KOH	205	10	32
Ni nanopowders	1M KOH	270	20	33
Ni NPs @ MWCNTs	1M KOH	220	20	34
NiP_2 @ carbon cloth	1M KOH	102	10	35
CoS/NC@MoS_2 composites	0.5 M H_2SO_4	77	10	36

In order to further evaluate effect of the Co doping and rGO composition on the electrocatalytic activity, the Tafel plots (Fig. 4b) of the samples derived from the LVS polarization curves. The corresponding Tafel slopes of MoS_2, Co-MoS_2, rGO-5-Co-MoS_2, rGO-10-Co-MoS_2 and rGO-20-Co-MoS_2 are 147, 146, 145, 140 and 149 mV dec^{-1}, respectively. The smaller Tafel slope exhibits a preferable reaction kinetics in the HER process for rGO-10-Co-MoS_2. Fig. 5c shows the electrochemical impedance spectroscopy (EIS) curves of the MoS_2, Co-MoS_2, rGO-5-Co-MoS_2, rGO-10-Co-MoS_2 and rGO-20-Co-MoS_2, respectively. The charge transfer resistance (R_{ct}) can be calculated by fitting EIS curves using equivalent circuit (inset of Fig.4c). The R_{ct} values of MoS_2, Co-MoS_2, rGO-5-Co-MoS_2, rGO-10-Co-MoS_2 and rGO-20-Co-MoS_2 are 13137, 3780, 999.3, 495.2 and 6.62×10^{11} Ω, respectively. The rGO-10-Co-MoS_2 shows the lowest R_{ct} value, indicating the best electron conductivity and easier charge transfer at the electrode/electrolyte interface of rGO-10-Co-MoS_2 as compared with other samples, which are conducive to improve its electrocatalytic HER activity[31]. The long-term catalytic stability of rGO-10-Co-MoS_2 is measured by time-dependent current density curves. Fig. 4d presents the current-time curve of rGO-10-Co-MoS_2 catalyst. Slight decrease has been seen for the current density. This result indicate that the sample of rGO-10-Co-MoS_2 exhibits the outstanding HER catalytic stability for 6h. The rGO-10-Co-MoS_2 represents excellent electrocatalytic activity for HER and stability, which could be explained as below: i) conductive cobalt its sulfide could effectively reduce the

internal resistance and interface resistance between electrode and electrolyte. ii) Coupling of rGO and MoS_2 will be conducive to produce more electronic transmission channels and active sites.

4. CONCLUSION

In summary, rGO-Co-MoS_2 composites were synthetized via one-step hydrothermal method. The rGO-Co-MoS_2 composites exhibit good electrocatalytic activity and stability in the acid condition for HER. The rGO-10-Co-MoS_2 presents the lowest overpotentials of 205 mV at a current density of 10 mA cm^{-2} and the smallest Tafel slope. The rGO-10-Co-MoS_2 shows little change of current density after 6h. The results indicated that cobalt doping and rGO hybrid is a effective method to improve electrocatalytic activity for HER.

ACKNOWLEDGEMENTS
This work was supported by National Natural Science Foundation of China (Nos. 51701001, 61804039, 51802145), Academic funding projects for Top Talents in Subjects (Majors) of Universities (No. gxbjZD31), Natural Science Foundation of Anhui Higher Education Institution of China (KJ2019A0734, KJ2017A924, KJ2017A002, KJ2019A0735), Natural Science Foundation of Anhui Province (No. 1808085QE126) and Foundation of Co-operative Innovation Research Center for Weak Signal-Detecting Materials and Devices Integration Anhui University (No. Y01008411, WRXH201703).

References

1. T.Y. Chen, Y.H. Chang, C.L. Hsu, K.H. Wei, C.Y. Chiang, L.J. Li, *Int. J. Hydrogen. Energ.*, 38(2013)12302.
2. Z. Bai, S. Li, J. Fu, Q. Zhang, F. Chang, L. Yang, J. Lu, Z. Chen, *Nano Energy*, 58(2019)680.
3. X. Chen, K. Zhang, Z. An, L. Wang, Y. Wang, S. Sun, T. Guo, D. Zhang, Z. Xue, X. Zhou, X. Lu, *Int. J. Hydrogen. Energ.*, 43(2018)7326.
4. J. Li, S. Yang, J. Liu, Y. Zhuang, Y. Tian, Q. Hu, Z. Xu, L. Wang, F. Li, *J. Alloy Compd.*, 786(2019)377.
5. C. Li, B. Zhang, Y. Li, S. Hao, X. Cao, G. Yang, J. Wu, Y. Huang, *Appl. Catal. B-En.,* 244(2019)56.
6. K.H. Ruiz, J. Liu, R. Tu, M. Li, S. Zhang, J.R. Vargas Garcia, S. Mu, H. Li, T. Goto, L. Zhang, *J. Alloy Compd.,* 747 (2018) 100.
7. L.Hu, X.F. Song, S.L. Zhang, H.B. Zeng, X.J. Zhang, R. Marks, D. Shan, *J. Catal.,* 366 (2018) 8.
8. G.Q. Huang, Y.F. Yan, J. Wu, Y.F. Shen, A.P. Gerlich, *J. Alloy Compd.,* 786(2019)257.
9. J. Dong, X. Zhang, J. Huang, S. Gao, J. Mao, J. Cai, Z. Chen, S. Sathasivam, C.J. Carmalt, Y. Lai, *Electrochem. Commun.,* 93(2018)152.
10. C. Du, H. Huang, J. Jian, Y. Wu, M. Shang, W. Song, *Appl. Catal. A-Gen.,* 538(2017)1.
11. Z. Qiu, Y. Peng, D. He, Y. Wang, S. Chen, J Mater Sci, 53(2018)12322.
12. J. Feng, H. Zhou, J. Wang, T. Bian, J. Shao, A. Yuan, *Int. J. Hydrogen Energ.,* 43(2018)20538.
13. P.H. Gao, B.Y. Chen, W. Wang, H. Jia, J.P. Li, Z. Yang, Y.C. Guo, *Surf. Coat. Tech.,* 363(2019)379.
14. E. Girel, E. Puzenat, C. Geantet, P. Afanasiev, *Catal. Today,* 292(2017)154-163
15. X. Wu, H. Zhang, Z. Ma, T. Tao, J. Gui, W. Song, B. Yang, H. Zhang, *J. Alloy Compd.,* 786 (2019) 205.
16. Z. Wu, M. Song, J. Wang, Q. Li, S. Wang, X. Liu, *J. Alloy Compd.,* 786(2019)475.
17. C. Zhang, L. Jiang, Y. Zhang, J.Hu, M.K.H. Leung, *J. Catal.,* 361(2018)384.
18. K. Zhao, W. Gu, L. Zhao, C. Zhang, W. Peng, Y. Xian, *Electrochim. Acta,* 169(2015)142.
19. X. Zhang, S. Liu, Y. Zang, R. Liu, G. Liu, G. Wang, Y. Zhang, H. Zhang, H. Zhao, *Nano Energy,*

30(2016)93.
20. W.H. Hu, G.Q. Han, F.N. Dai, Y.R. Liu, X. Shang, B. Dong, Y.M. Chai, Y.Q. Liu, C.G. Liu, *Int. J. Hydrogen Energ.,* 41 (2016) 294.
21. S. Hua, D. Qu, L. An, G. Xi, G. Chen, F. Li, Z. Zhou, Z. Sun, *Chinese J. Catal.,* 38(2017)1028.
22. D. Wang, X. Zhang, Y. Shen, Z. Wu, *RSC Adv.,* 6(2016)16656.
23. Z. Pan, Z. Xia, Y. Tao, X. Shen, *Catalysis Commun.,* 125 (2019) 56.
24. Z.Q. Cao, M.Z. Wu, H.B. Hu, G.J. Liang, C.Y. Zhi, *NPG Asia Mater.,* 10(2018)670.
25. L. Yin, X. Hai, K. Chang, F. Ichihara, J. Ye, *Small,* 14(2018)1704153.
26. H. Li, X. Qian, C. Xu, S. Huang, C. Zhu, X. Jiang, L. Shao, L. Hou, *ACS Applied Materials & Interfaces,* 9(2017)28394.
27. A.P. Wu, C.G. Tian, H.J. Yan, Y.Q. Jiao, Q. Yan, G.Y. Yang and H.G. Fu, *Nanoscale,* 8(2016)11051.
28. X. Guo, W. Zhang, D. Zhang, S. Qian, X. Tong, D. Zhou, J. Zhang, A. Yuan, *ChemElectroChem,* 6 (2019) 62019.
29. R. Liu, H. Zhang, X. Zhang, T. Wu, H. Zhao, G. Wang, *RSC Adv.,* 7(2017)19181.
30. X.B. Xiang, Y. Yu， W. Wen and J.M. Wu, *New J. Chem.,* 42(2018)265.
31. S.A. Shah, X. Shen, M. Xie, G. Zhu, Z. Ji, H. Zhou, K. Xu, X. Yue, A. Yuan, J. Zhu, Y. Chen, *Small,* 15(2019)1804545.
32. Y. Xu, W. Tu, B.W. Zhang, S.M. Yin, Y.Z. Huang, M. Kraft, R. Xu, *Adv. Mater.,* 29(2017)1605957.
33. J.R. McKone, B.F. Sadtler, C.A. Werlang, N.S. Lewis and H.B. Gray, *ACS Catal.,* 3(2013)166.
34. M.A. McArthur, L.Jorge, S.Coulombe and S.Omanovic, *J. Power Sources,* 266(2014)365.
35. P. Jiang, Q. Liu and X. Sun, *Nanoscale,* 6 (2014)13440.
36. Y.Y. Zhao, M.F. Bi, F.F. Qian, P.Y. Zeng, M.N. Chen, R.J. Wang, Y.Y. Liu, Y. Ding, Z. Fang, *ChemElectroChem,* 5(2018)3953.